Journal Pre-proof

Comparison of structural, electronic and magnetic properties in nickel-doped graphene containing different pyridinic-N coordination

H. Cabrera-Tinoco, L. Borja-Castro, R. Valencia-Bedregal, A. Perez-Carreño, J. Albino Aguiar, N.O. Moreno, S.N. Holmes, C.H.W. Barnes, L. De Los Santos Valladares

PII: S2352-4928(24)02085-3

DOI: https://doi.org/10.1016/j.mtcomm.2024.110104

Reference: MTCOMM110104

To appear in: *Materials Today Communications*

Received date: 23 April 2024
Revised date: 31 July 2024
Accepted date: 9 August 2024

Please cite this article as: H. Cabrera-Tinoco, L. Borja-Castro, R. Valencia-Bedregal, A. Perez-Carreño, J. Albino Aguiar, N.O. Moreno, S.N. Holmes, C.H.W. Barnes and L. De Los Santos Valladares, Comparison of structural, electronic and magnetic properties in nickel-doped graphene containing different pyridinic-N coordination, *Materials Today Communications,* (2024) doi:https://doi.org/10.1016/j.mtcomm.2024.110104

Comparison of structural, electronic and magnetic properties in nickel-doped graphene containing different pyridinic-N coordination

H. Cabrera-Tinoco[a(*)], L. Borja-Castro[b], R. Valencia-Bedregal[b], A. Perez-Carreño[a], J. Albino Aguiar[c], N.O. Moreno[d], S.N. Holmes[e], C.H.W. Barnes[f], L. De Los Santos Valladares[c,f(*)]

[a] Área de Ciencias Básicas, Universidad Continental, Lima 15311, Perú.
[b] Laboratorio de Cerámicos y Nanomateriales, Facultad de Ciencias Físicas, Universidad Nacional Mayor de San Marcos, Ap. Postal 14-0149, Lima, Perú.
[c] Programa de Pós-Graduação em Ciências de Materiais, Centro de Ciências Exatas e da Natureza, Universidade Federal de Pernambuco, 50670-901 Recife-PE, Brazil.
[d] Departamento de Física, Universidade Federal de Sergipe, São Cristóvão, SE 49100-000, Brazil
[e] Department of Electronic and Electrical Engineering, University College London, Torrington Place, London WC1E 7JE, UK.
[f] Cavendish Laboratory, Department of Physics, University of Cambridge, J. J Thomson Ave., Cambridge CB3 0H3, UK.

(*) Corresponding authors emails: Hcabrera@continental.edu.pe (H. Cabrera-Tinoco) and ld301@cam.ac.uk (L. De Los Santos Valladares)

Abstract

Recently, single-atom catalysts (SAC) have shown to be an alternative to enable chemical reactions related to the generation of renewable energy and to control environmental pollution. These SACs can be synthesized by modifying the structure of a substrate such as graphene through doping with single transition metal atoms. One of the possible ways to improve its catalytic properties is to modify the coordination of the metal atom with pyridinic-N sites. Thus, understanding the properties of the material when the coordination is modified is crucial for potential applications. In the present work, the electronic, structural and magnetic properties of a graphene sheet doped with a nickel atom were studied by computational simulation using DFT. These properties were inspected by changing the coordination of the nickel atom with pyridinic-N sites. A ~0.3 eV gap is found when graphene is doped with the nickel atom and it is maintained with the modification of the coordination, except for the substrate with three nitrogen atoms. A change in the chemical nature of the bond between the Ni atom and its neighbours from a pi to a sigma type is also revealed.

Keywords: Graphene-based support; Density functional theory; Ni-doped crystal orbital Hamilton population; Pyridinic-N

1 Introduction

Research on climate change impacts and the generation of renewable energy are very important topic. Today for multiple different reasons, such as the increasing demand of energy, vulnerability of the natural resources, pollution, and to the continuous development of methodologies and availability of data. In this way, water splitting [1] and CO_2 conversion [2] are processes which are very well related to climate change and renewable energy topics. Specifically, these processes are based on a series of chemical reactions such as oxygen reduction reaction (ORR), hydrogen evolution reaction (HER), oxygen evolution reaction (OER), CO_2 reduction reaction (CO_2RR), among others. The OER and HER mentioned above present high overpotential characteristics, which constitutes a barrier to the generation of renewable energy [3,4]. In the case of CO_2RR, the

activation energy is quite large. This is because CO_2 is a very stable molecule, i.e the dissociation energy of the C=O bond (750 KJ mol^{-1}) is greater than that of other bonds such as C-O (327 KJ mol^{-1}), C-C (336 KJ mol^{-1}) or C-H (441 KJ mol^{-1}) [5].That is the reason why it is necessary to search for novel materials that can catalyse these reactions.

On the other hand, graphene is a material that has been intensively studied during the recent decades because of its interesting electronic and mechanical properties. It has been reported that the exfoliation of graphite results in oxidation processes and generation of atomic defects in its structure [6,7]. These defects can be replaced by transition metals in order to increase the chemical activity in these sites. These materials are also known as single atom catalysts (SAC) [7,8]. Recently, interest has been generated in SACs due to advantages such as their charge transfer kinetics, the synergy between graphene and the metal atom, among others [9]. The synthesis and characterization of SACs could be quite complex due to the large number of variables that can influence their physical and chemical properties. For example, modification in the coordination of the metal atom by pyridinic-N sites improves the chemical activity of the SACs. Moreover, it has been recently reported that CO_2 adsorption improves when the number of pyridinic-N sites on the graphene sheet doped with an iron atom is increased [10].

In order to better understand the possible catalytic processes, it is necessary to understand the electronic, structural and magnetic configurations of these substrates and how they change with change in coordination. This has not been explored in detail to our knowledge. In this work, these properties are studied in substrates formed by a graphene sheet doped with a nickel atom through computational calculations based on DFT. Furthermore, the coordination of the nickel atom was modified by replacing the neighbouring carbon atoms with nitrogen atoms, forming pyridine sites.

2 Simulation method and setup

In this article, the SIESTA program [11] was used to perform the calculations of structural relaxation and electronic structure of the substrates. The structure of the graphene sheet was relaxed from a 5×5 supercell (50 atoms). To describe the electronic behaviour, the generalized gradient approximation of Perdew, Burke and Ernzernhof (PBE) [12] was used. The electronic description was complemented with the use of norm-conserving pseudo-potentials that expands the eigenfunctions of the valence electrons with a double-ζ plus polarization functions as basis set (DZP). All calculations were done taking into account the spin polarization due to the presence of the Ni atom.

A vertical space of 20 Å was placed between each graphene sheet image to avoid interaction between them. Structural relaxation was carried out using the Conjugate Gradient algorithm (CG) until forces less than 0.01 eV/Å were obtained. Likewise, the limit variation of the total energy was 1 x 10^{-5} eV to stop the self-consistent cycles during this relaxation. To sample the Brillouin zone in the relaxation process, it was used a 7x7 k-points grid (Monkhorst-Pack scheme) and a 350 Ry of mesh cut-off. For the characterization of the electronic and magnetic properties, it was used a 8x8 k-points grid (Monkhorst-Pack scheme) and a 400 Ry of mesh cut-off.

The Projected Density of States (PDOS), the Crystal Hamilton Orbital Population (COHP) method [13], the integration of the COHP (ICOHP), the Bader charge analysis

[14] and total magnetic moment (TMM) are parameters used to study the electronics and magnetic characteristics of the computational models. The binding energy of the Nickel atom was calculated by

$$E_{bin} = E_{sub} - (E_{Ni} + E_{SVNx}) \quad (1),$$

where E_{sub}, E_{Ni} and E_{SVNx} are the total energy of the substrate (Ni-N0, Ni-N1, Ni-N2 or Ni-N3), the free iron atom and single vacancy graphene doped with x (x=0,1,2 and 3) nitrogen atoms, respectively. To better explore the interaction of potential adsorbents with the systems studied in this work, the d-band center defined by the following equation was used

$$\epsilon_d = \frac{\int_{-\infty}^{E_f} \epsilon \rho_d d\epsilon}{\int_{-\infty}^{E_f} \rho_d d\epsilon} \quad (2),$$

where ρ_d and E_F are the density of d-electrons density of states and the Fermi energy respectively.

3 Results and discussions

Table 1 shows data corresponding to the thermodynamic stability such as E_{bin}, structural characteristics and TMM of the substrates. In this table it can be seen that E_{bin} increases with the increase of the pyridinic-N sites in the coordination of the nickel atom. This has been reported in other works. For example, Gao and collaborators obtained -6.65 eV, -5.34 eV, -5.05 eV and -4.52 eV for the Ni-N0, Ni-N1, Ni-N2 and Ni-N3 systems respectively [15]. In a previous publication Gao achieved quite similar values -6.69 eV, -5.53 eV, -5.00 eV and -4.32 eV for Ni-N0, Ni-N1, Ni-N2 and Ni-N3 respectively [16]. As can be seen, these results are quite close to the values calculated by Gao. It should be noted that the only system that differs from the decreasing trend is Ni-N1. In the work of Krasheninnikov et al. a value close to -7 eV is obtained for E_{bin} in the case of Ni-N0 [17].

The structure has been also characterized in the present work. Fig. 1 shows the structures obtained from the relaxation process described in Section 2. As reported in various works, the substitution of a carbon atom for a different atom, in this case a transition metal, causes a distortion in the planar structure of graphene. The nickel atom rises above the plane of the graphene. It can be noticed that this height increases with the number of nitrogen atoms in the system. The height obtained in the literature has been 1.28 Å, 1.27 Å, 1.40 Å and 1.38 Å for Ni-N0, Ni-N1, Ni-N2 and Ni-N3 respectively [15,16]. Another important structural parameter related to the alteration of the structure of pristine graphene is the modification of the bond length between the Ni, C and N atoms. The bond length calculated between carbon atoms is 1.41 Å for the pristine graphene, which is in accordance with the literature [18]. Table 1 shows that the bond length between the nickel and carbon atoms increases to 1.83 Å for the Ni-N0 system. When pyridinic-N sites are added, this length increases to 1.84 Å and 1.87 Å for Ni-N1 and Ni-N2 respectively. In the case of the bond between the nickel and nitrogen atoms, the length is even greater than the Ni-C bonds. The bond length achieved was 1.91 Å (Ni-N1 and Ni-N3) or 1.92 Å (Ni-N2). The literature reports around 1.80 Å for the length of the Ni-C bond [17].

The charge variation of the nickel atom was analysed using Bader charge analysis [14]. It is shown that the nickel atom loses charge due to the interaction with neighbouring atoms and that this loss is accentuated with pyridinic-N coordination. Gao reports 0.50*e*, 0.60*e*, 0.70*e* and 0.77*e* for Ni-N0, Ni-N1, Ni-N2 and Ni-N3 respectively [15]. Note that the results in the present work slightly differ from the results calculated by Gao.

The fact that the binding energy increases despite the shared charge between the nickel atom and graphene seems contradictory. However, this is explained by the fact that the presence of nitrogen atoms destabilizes the structure of graphene, as previously shown by Kropp and collaborators [19]. This causes the binding energy to increase although it remains negative. This was also reported in the case of other transition metals such as iron [10]. On the other hand, the total spin moment is also reported. The TSP for the Ni-N0 system is zero because although Ni has ten valence electrons, it only has two unpaired electrons in 3d. This indicates that when interacting with the three neighbouring carbon atoms, the 4s electrons and the two 3d unpaired electrons form three sigma bonds and one pi bond, so the magnetization is zero. When a nitrogen atom is introduced, an electron is added, which is why Ni-N1 has a magnetization of $1\mu_B$. For Ni-N2, the system converges to a kind of triplet state where there are two unpaired states, consequently a magnetization of $2\mu_B$. In the case of Ni-N3, a doublet state would be expected however the magnetization exceeds $1\mu_B$. The reason will be discussed in detail when analysing the electronic structure and chemical interactions.

Table 1. Binding energy (E_{bin}), height of the Ni atom (h), Ni-C bond length (d_{Ni-C}), Ni-N bond length (d_{Ni-N}), charge variation of the Ni atom and total magnetic moment (TMM)

Substrate	E_{bin} (eV)	h (Å)	d_{Ni-C} (Å)	d_{Ni-N} (Å)	Δq_{Ni} (e)	TMM (μ_B)
Ni-N0	-6.59	1.60	1.83	-	0.60	0.00
Ni-N1	-4.62	1.66	1.84	1.91	0.73	1.00
Ni-N2	-5.43	1.71	1.87	1.92	0.84	1.99
Ni-N3	-4.70	1.66	-	1.91	0.89	1.71

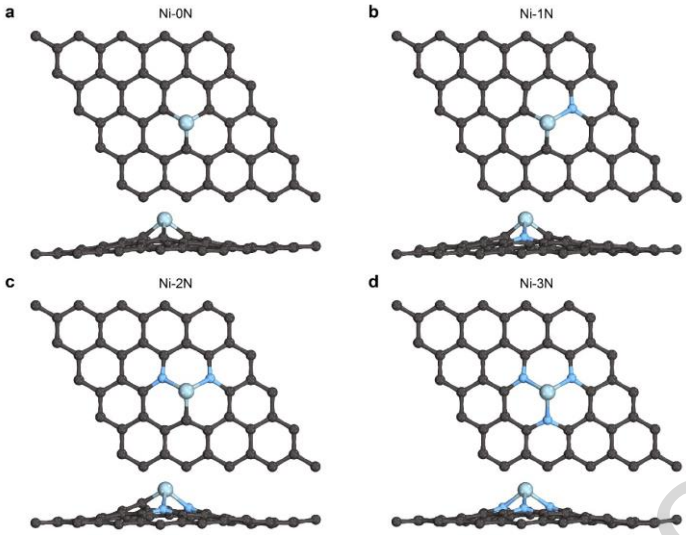

Fig. 1. Relaxed structures of Ni-N0, Ni-N1, Ni-N2 and Ni-N3.

Fig. 2 shows the band structures of the majority and minority states of all substrates. As seen in Table 1, the magnetization of Ni-N0 is zero, so the majority and minority bands are equal (see Fig. 2a,b). In the band structure, the four bands close to the Fermi energy draw attention. The Dirac cone structure of graphene is lost to give rise to a gap of approximately 0.3 eV. The bands furthest from the Fermi energy present some dispersion near K, these bands correspond to the $2p_z$ orbitals of the carbon atom, which is why their dispersion is due. The other two bands correspond to almost degenerate states of the 3d orbitals of the nickel atom, and they are also flat bands. This indicates that these orbitals are localized in the vacancy region. The rest of the Ni 3d bands are well below the Fermi energy, which indicates that these orbitals must be forming sigma bonds with carbon atoms. Ni 4s orbitals are above the Fermi energy. This would show that the electrons of Ni 4s form bonds with an ionic nature with the carbon atoms. The band structure shown in Fig. 1a,b is quite similar to the results calculated by Santos et al [20].

In the case of Ni-N1, since the magnetization is not zero, then the majority and minority bands are different. It can be seen in the majority states that the 3d Ni orbitals are well below the Fermi energy. The band with 3d Ni states closest to the Fermi energy is just above -1 eV (see Fig. 2c,d). The minority states are somewhat closer to the Fermi energy. Although the most notable difference is the presence of the flat bands that, in the case of Ni-N1, are no longer related to degenerate states and the spacing between these bands is almost 0.3 eV. In this case the Ni 4s states, as in Ni-N0, are above the Fermi energy. The Ni-N2 system is quite similar to Ni-N1 (see Fig. 2e,f). The difference is that in the case of Ni-N2, the Ni 3d bands are even further below the Fermi energy. The flat bands also move further upward from the Fermi energy and become degenerate again. However, the separation almost does not change between the valence and conduction bands. As expected, there are more bands corresponding to N 2p (orange colour). Finally, the case of Ni-N3 is particular. Finally, the case of Ni-N3 is particular. In this case the Dirac point moves below the Fermi energy. Furthermore, unlike the other substrates, the Ni 4s bands appear flat for the majority states. In the case of minority states, a downward shift in the bands is also observed. The flat Ni 3d band states lie almost above the Fermi energy.

In Fig. 2 it is also possible to observe the presence of flat bands. The flat bands closest to the Fermi energy are above E_F and are associated with the 3 d orbitals of the nickel atom as can be seen in Fig. 2a,b,c,d,f,h. As is known, the flat bands are associated with the spatial localization of the related electrons [21]. In that sense we can infer that the Ni 3d electrons are spatially localized in the dopant region. This is an indication of a strong interaction between the Ni atom and the neighbouring atoms. These flat bands were also observed by Santos et. al. in the case of the Ni-N0 system [20].

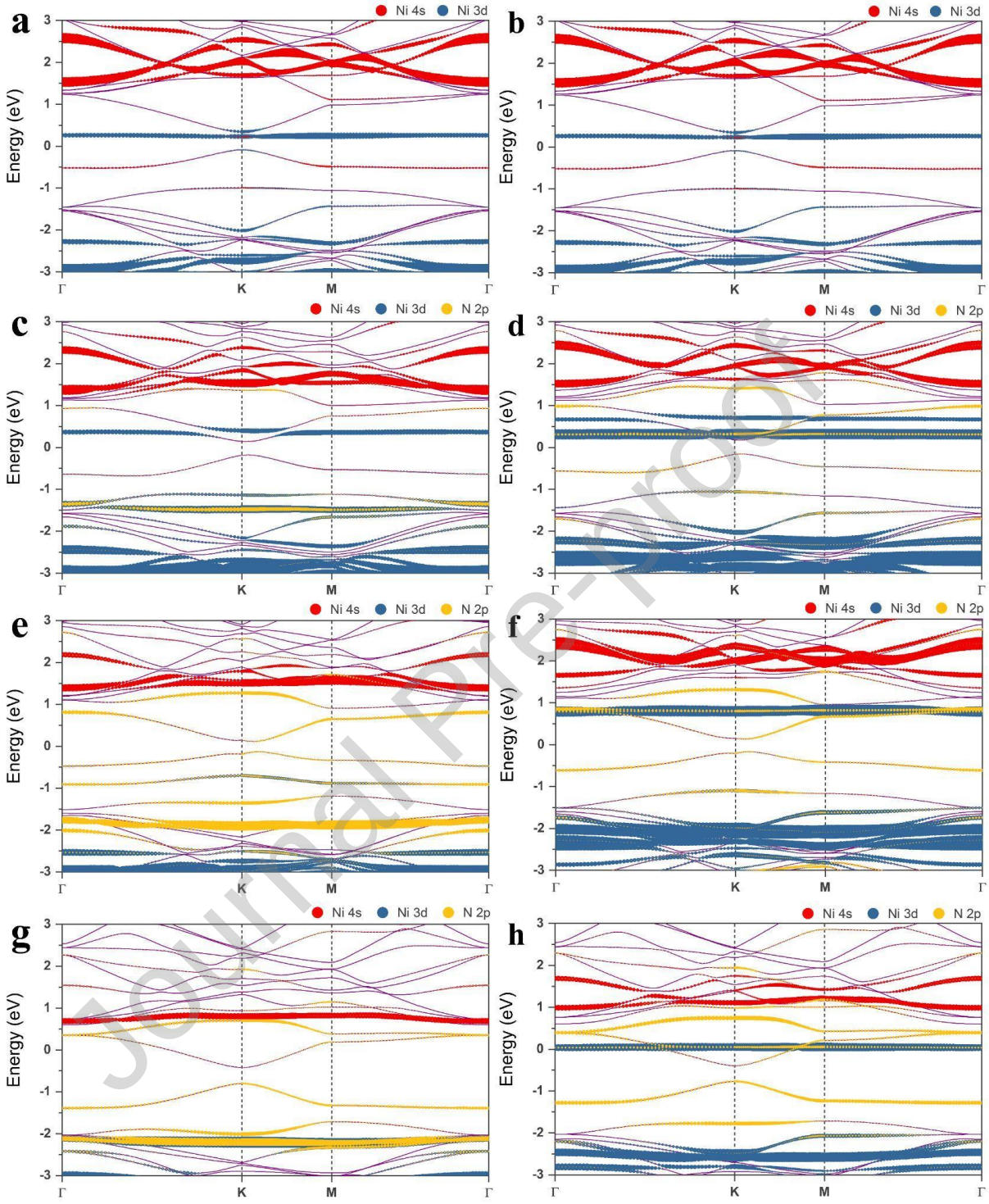

Fig. 2. Structure of majority (a) and minority (b) bands of Ni-N0, majority (c) and minority (d) bands of Ni-N1, majority (a) and minority (b) bands of Ni-N2, and majority (a) and minority (b) bands of Ni-N3.

Fig. 3 shows the projected density of states of all the systems. In the case of Ni-N0, the majority and minority states are equal. This is to be expected since the magnetization is zero. As had been mentioned in the analysis of the band structure, it was observed 3d Ni states were located near the Fermi energy. A strong hybridization is also observed between the orbitals of the nickel atom and the 2p orbitals of the carbon atom. This is

inferred from noting that the C 2p states coincide with the Ni 3d states (see Fig. 3a). When one more electron is added due to the substitution of a carbon atom for a nitrogen atom (Ni-N1), the symmetry between the majority and minority states is lost in the case of the Ni 3d orbitals. This can be seen in Fig. 3b. As expected, it is the Ni 3d orbitals that generate the difference between the majority and minority PDOS. The unoccupied Ni 3d state at 0.36 eV draws attention due to the high hybridization with the C 2p orbitals. This high hybridization is lost in the case of Ni-N2 and Ni-N3. The unoccupied majority Ni 3d state which is present close to E_F in Ni-N0 and Ni-N1 is not present in Ni-N2 and Ni-N3. It should be noted that in the case of Ni-N3, the bands show a downward shift in the Fermi energy. Which can also be seen in Fig. 3d. The minority unoccupied state of Ni 3d is always maintained in all systems. In the case of Ni-N3 this state is almost above E_F.

The way in which the studied systems interact with potential adsorbents can be predicted through the d band center. It is understood that when the value of the d band center is closer to the Fermi energy, it would indicate a better adsorption and therefore there would be a tendency to improve its catalytic properties [22]. The d band centers of each system were calculated through Eq. 2. The distances between the value of the d band center and the Fermi energy were $3.74\ eV$, $3.48\ eV$, $3.22\ eV$ and $3.50\ eV$ for Ni-N0, Ni-N1, Ni-N2 and Ni-N3 respectively. This would indicate a non-monotonic improvement in the catalytic properties of the substrates as the pyridinic-N sites increase.

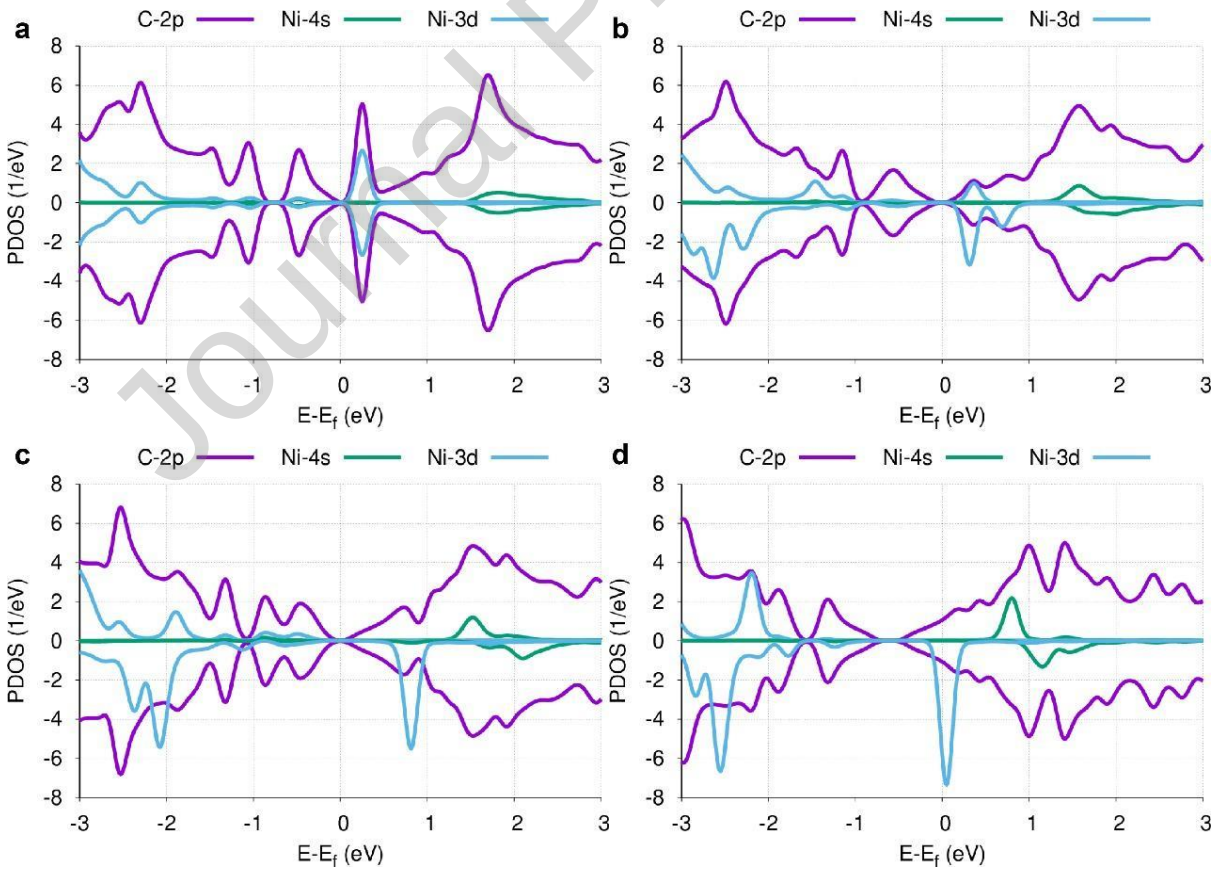

Fig. 3. Projected density of states (PDOS) of Ni-N0, Ni-N1, Ni-N2 and Ni-N3.

Fig. 4 shows the COHP curves of the most important orbital pairs of the substrates. In Fig. 4a, the hybridization between the orbitals of the nickel and carbon atom can be observed. It can be noted that the Ni 4s-C 2p interaction is basically anti-bonding, because most of the peaks have negative values. The Ni 4s-C 2s orbital is shown as a nonbonding type orbital pair because it is almost zero in the entire energy range except for the states between 1.5 eV and 2.5 eV. It is noteworthy that the spatially localized states related to the flat bands shown in Fig. 2 are antibonding states as shown in Fig. 4. This would imply that the nickel atom stabilizes the substrate structure by shifting these states above the Fermi energy. Table 2 indicates that the main orbital pairs for this system are Ni 3d-C 2p and Ni 4s-C 2p, which represent 64.6% and 35.4% of the Ni-C bond respectively. The Ni-N1 system has a majority bonding state related to the Ni 4s-C 2p orbital pair at -1.5 eV (see Fig. 4b). Then the other majority states are of the anti-bonding type. Most of the minority states are antibonding with the exception of the Ni 3d-C 2p orbital pair, which has bonding states with energies lower than -2.5 eV. From Table 2 it is noted that the main orbital pairs are Ni 3d-C 2p and Ni 4s-C 2p with 47.6% and 26.7% respectively. In the case of Ni-N2, the Ni 4s-C 2p orbital pair presents bonding majority states in energy ranges closer to the Fermi energy. These bonding states correspond to the Ni4s-C2p orbital pair. The minority states are bonding at energies lower than -2.5 eV (see Fig. 4c). These bonding states are related to pair orbitals Ni4s-C2p, Ni3d-C2p and Ni3d-N2p. According to Table 2, the most important orbital pairs are Ni4s-C2p, Ni3d-C2p and Ni3d-N2p with 37.6%, 23.1% and 21.5% participation in the Ni-C and Ni-N interaction respectively. Finally, up to three antibonding peaks at −2.25 eV, −1.15 eV, and 1 eV are shown in Fig. 4 d. These three peaks correspond to majority states of the Ni 4s-N 2s and Ni 4s-N 2p orbital pairs. The minority states present antibonding states with an exception of the Ni 4s-N 2p orbital pair at energies lower than -2.5 eV. Table 2 indicates that the orbital pairs that contribute the most to the Ni-N bond are Ni4s-N2p and Ni3d-N2p with 65.6% and 34.4%.

Table 2. ICOHP values of the main orbital pairs in the substrates.

Substrate	Orbital-pairs	ICOHP (eV)	Percentage (%)
Ni-0N	Ni3d-C2p	-0.2792	64.6
	Ni4s-C2p	-0.1533	35.4
Ni-1N	Ni3d-C2p	-0.1746	47.6
	Ni4s-C2p	-0.0980	26.7
	Ni4s-N2p	-0.0617	16.8
	Ni3d-N2p	-0.0325	8.9
Ni-2N	Ni4s-N2p	-0.1120	37.6
	Ni3d-C2p	-0.0690	23.1
	Ni3d-N2p	-0.0640	21.5
	Ni4s-C2p	-0.0532	17.8
Ni-3N	Ni4s-N2p	-0.1815	65.6

Ni3d-N2p	-0.0951	34.4

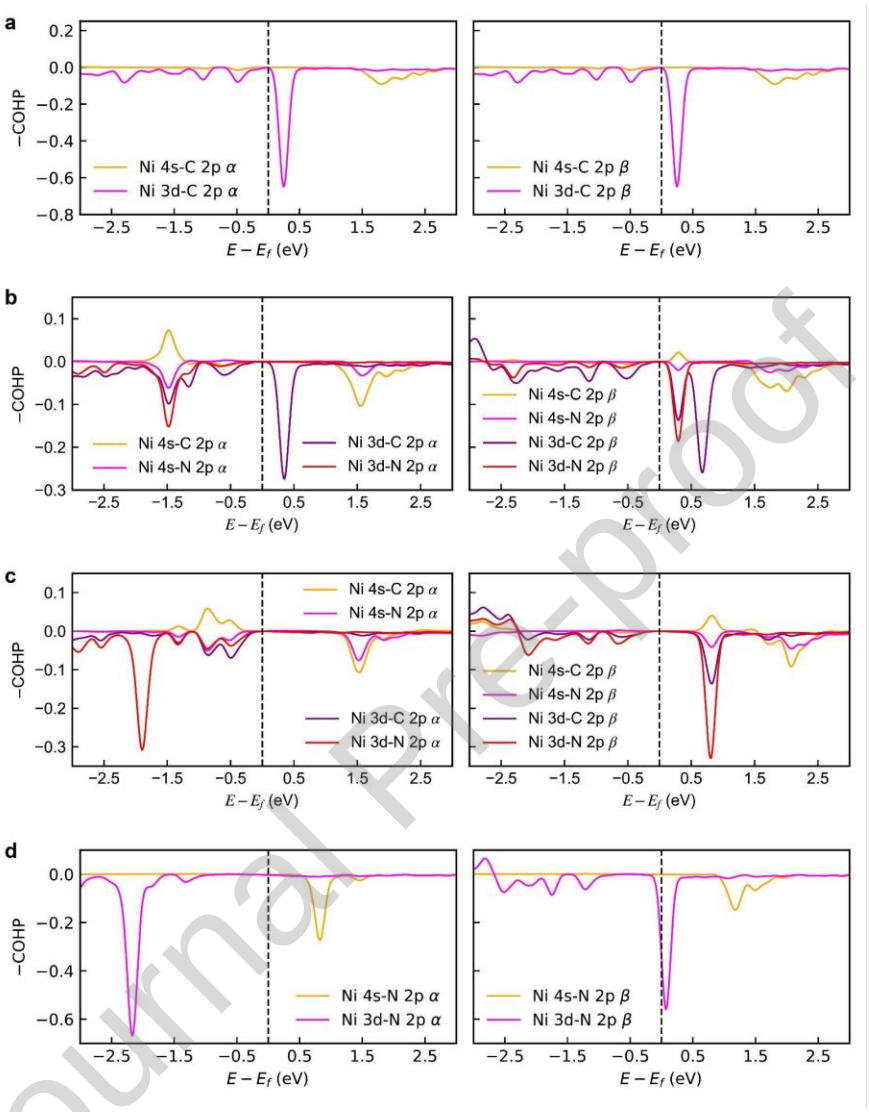

Fig. 4. Crystal orbital Hamilton population (COHP) curves of the main orbital pairs in Ni-N0 (a), Ni-N1 (b), Ni-N2 (c) and Ni-N3 (d).

An important issue is that the chemical model used in this work in principle does not explicitly take correlation or self-interaction effects into account. One way to correct is to use methods such as GGA+U, which consists of adding a term to the energy that depends on the matrix density of the electrons in which a strong Coulomb repulsion is expected, such as the 3d electrons of the nickel atom [23]. This term is graded by the parameter $U_{eff} = \bar{U} - \bar{J}$. However, this does not mean that the PBE functional is a bad model since other works show that the results of its investigations vary little using the GGA + U method [24,25]. In this work, the GGA+U method with $U_{eff} = 1$ and $3\ eV$ was used to verify the effect on the electronic properties of the Ni-N0 and Ni-N3 substrates. The results can be seen in Fig. S1 where the band structures are shown. In Fig. S1a,b it can be noted that the variation in relation to Fig. 2a,b is minimal for $U_{eff} = 1\ eV$ and $U_{eff} = 3\ eV$. The increase in the value of U_{eff} does not imply a modification of TMM, which remains zero. In the case of Ni-N3, a TMM of 1.80 μ_B and

2.03 μ_B is observed for $U_{eff} = 1\ eV$ and $U_{eff} = 3\ eV$ respectively. However, the band structures remain almost invariant in relation to Fig. 2g,h (see Fig. S1c,d,e,f). This leads to the inference that the results do not change significantly with the differentiated treatment of the 3d Ni electrons.

4 Conclusions

The structural, electronic and magnetic properties of a nickel-doped graphene sheet were studied and compared with the number of pyridinic-N sites. The structural characteristics presented in this work are reasonable and agree with those reported in the literature. The fact that the planar structure of graphene is altered when doped with a transition metal such as nickel and it increases with pyridinic-N coordination confirms the literature reports. The electronic structure shows the generation of a band gap of 0.3 eV around the Dirac point when the pyridine sites are introduced. This separation disappears in Ni-N3 in which the conduction band shifts to lower energies. The magnetic properties reported in the present work follow the expected order of the electronic distribution. Zero magnetization in the case of Ni-N0 has been widely reported in the literature and agrees well with the presented results. When modifying the coordination, attention is drawn to the magnetization of the Ni-N2 and Ni-N3 systems, which take on values that must be explored more widely in subsequent work.

Acknowledgements
The work at the Universidade Federal de Pernambuco, Brazil has been supported by the PROFESSOR VISITANTE Program Nº. 13/2022, Contract No. 062 /2022 (Process no. 23076.101469/2021-69).

Authors Contribution:

Data acquisition, methodology, data curation and formal analysis (H. Cabrera-Tinoco, L. Borja-Castro, R. Valencia-Bedregal and L. De Los Santos Valladares), conceptualization, interpretation, validation, data curation and visualization (A. Perez-Carreño, J. Albino Aguiar, N.O. Moreno, S.N. Holmes, C.H.W. Barnes and L. De Los Santos Valladares) and all authors have contributed to write and correct the manuscript.

References

[1] H. Idriss, Hydrogen production from water: past and present, Curr. Opin. Chem. Eng. 29 (2020) 74–82. https://doi.org/10.1016/j.coche.2020.05.009.
[2] Z. Sun, T. Ma, H. Tao, Q. Fan, B. Han, Fundamentals and Challenges of Electrochemical CO2 Reduction Using Two-Dimensional Materials, Chem 3 (2017) 560–587. https://doi.org/10.1016/j.chempr.2017.09.009.
[3] N.-T. Suen, S.-F. Hung, Q. Quan, N. Zhang, Y.-J. Xu, H.M. Chen, Electrocatalysis for the oxygen evolution reaction: recent development and future perspectives, Chem. Soc. Rev. 46 (2017) 337–365. https://doi.org/10.1039/C6CS00328A.
[4] S. Wang, A. Lu, C.-J. Zhong, Hydrogen production from water electrolysis: role of catalysts, Nano Converg. 8 (2021) 4. https://doi.org/10.1186/s40580-021-00254-x.
[5] Y. Wang, D. He, H. Chen, D. Wang, Catalysts in electro-, photo- and photoelectrocatalytic CO2 reduction reactions, J. Photochem. Photobiol. C Photochem. Rev. 40 (2019) 117–149. https://doi.org/10.1016/j.jphotochemrev.2019.02.002.

[6] H. Cho, I. Oh, J. Kang, S. Park, B. Ku, M. Park, S. Kwak, P. Khanra, J. Hee Lee, M. Jong Kim, Catalyst and doping methods for arc graphene, Nanotechnology 25 (2014) 445601. https://doi.org/10.1088/0957-4484/25/44/445601.
[7] Q. Zhang, X. Zhang, J. Wang, C. Wang, Graphene-supported single-atom catalysts and applications in electrocatalysis, Nanotechnology 32 (2021) 032001. https://doi.org/10.1088/1361-6528/abbd70.
[8] C. Pan, S. El-khodary, S. Wang, Q. Ling, X. Hu, L. Xu, S. Zhong, Research progress in graphene based single atom catalysts in recent years, Fuel Process. Technol. 250 (2023) 107879. https://doi.org/10.1016/j.fuproc.2023.107879.
[9] Y. Dai, F. Kong, X. Tai, Y. Zhang, B. Liu, J. Cai, X. Gong, Y. Xia, P. Guo, B. Liu, J. Zhang, L. Li, L. Zhao, X. Sui, Z. Wang, Advances in Graphene-Supported Single-Atom Catalysts for Clean Energy Conversion, Electrochem. Energy Rev. 5 (2022) 22. https://doi.org/10.1007/s41918-022-00142-w.
[10] H. Cabrera-Tinoco, L. Borja-Castro, R. Valencia-Bedregal, A. Perez-Carreño, A. Lalupu-García, I. Veliz-Quiñones, A.G. Bustamante Dominguez, C.H.W. Barnes, L. De Los Santos Valladares, Pyridinic-N Coordination Effect on the Adsorption and Activation of CO_2 by Single Vacancy Iron-Doped Graphene, Langmuir 40 (2024) 6703–6717. https://doi.org/10.1021/acs.langmuir.3c03327.
[11] A. García, N. Papior, A. Akhtar, E. Artacho, V. Blum, E. Bosoni, P. Brandimarte, M. Brandbyge, J.I. Cerdá, F. Corsetti, R. Cuadrado, V. Dikan, J. Ferrer, J. Gale, P. García-Fernández, V.M. García-Suárez, S. García, G. Huhs, S. Illera, R. Korytár, P. Koval, I. Lebedeva, L. Lin, P. López-Tarifa, S.G. Mayo, S. Mohr, P. Ordejón, A. Postnikov, Y. Pouillon, M. Pruneda, R. Robles, D. Sánchez-Portal, J.M. Soler, R. Ullah, V.W. Yu, J. Junquera, Siesta: Recent developments and applications, J. Chem. Phys. 152 (2020) 204108. https://doi.org/10.1063/5.0005077.
[12] J.P. Perdew, K. Burke, M. Ernzerhof, Generalized gradient approximation made simple, Phys. Rev. Lett. 77 (1996) 3865–3868. https://doi.org/10.1103/PhysRevLett.77.3865.
[13] S. Steinberg, R. Dronskowski, The crystal orbital hamilton population (COHP) method as a tool to visualize and analyze chemical bonding in intermetallic compounds, Crystals 8 (2018) 225. https://doi.org/10.3390/cryst8050225.
[14] G. Henkelman, A. Arnaldsson, H. Jónsson, A fast and robust algorithm for Bader decomposition of charge density, Comput. Mater. Sci. 36 (2006) 354–360. https://doi.org/10.1016/j.commatsci.2005.04.010.
[15] Z. Gao, A. Li, X. Li, X. Liu, C. Ma, J. Yang, W. Yang, H. Li, The adsorption and activation of oxygen molecule on nickel clusters doped graphene-based support by DFT, Mol. Catal. 477 (2019) 110547. https://doi.org/10.1016/j.mcat.2019.110547.
[16] Z. Gao, A. Li, X. Liu, C. Ma, X. Li, W. Yang, X. Ding, Density functional study of the adsorption of NO on Ni (n = 1, 2, 3 and 4) clusters doped functionalized graphene support, Appl. Surf. Sci. 481 (2019) 940–950. https://doi.org/10.1016/j.apsusc.2019.03.186.
[17] A.V. Krasheninnikov, P.O. Lehtinen, A.S. Foster, P. Pyykkö, R.M. Nieminen, Embedding Transition-Metal Atoms in Graphene: Structure, Bonding, and Magnetism, Phys. Rev. Lett. 102 (2009) 126807. https://doi.org/10.1103/PhysRevLett.102.126807.
[18] P. Rani, V.K. Jindal, Designing band gap of graphene by B and N dopant atoms, RSC Adv 3 (2013) 802–812. https://doi.org/10.1039/C2RA22664B.
[19] T. Kropp, M. Mavrikakis, Transition Metal Atoms Embedded in Graphene: How Nitrogen Doping Increases CO Oxidation Activity, ACS Catal. 9 (2019) 6864–6868. https://doi.org/10.1021/acscatal.9b01944.
[20] E.J.G. Santos, A. Ayuela, S.B. Fagan, J. Mendes Filho, D.L. Azevedo, A.G. Souza Filho, D. Sánchez-Portal, Switching on magnetism in Ni-doped graphene: Density functional calculations, Phys. Rev. B 78 (2008) 195420. https://doi.org/10.1103/PhysRevB.78.195420.
[21] Y. Chen, J. Huang, K. Jiang, J. Hu, Decoding flat bands from compact localized states, Sci. Bull. 68 (2023) 3165–3171. https://doi.org/10.1016/j.scib.2023.11.032.
[22] A.J. Medford, A. Vojvodic, J.S. Hummelshøj, J. Voss, F. Abild-Pedersen, F. Studt, T. Bligaard, A. Nilsson, J.K. Nørskov, From the Sabatier principle to a predictive theory of transition-metal heterogeneous catalysis, J. Catal. 328 (2015) 36–42. https://doi.org/10.1016/j.jcat.2014.12.033.

[23] S.L. Dudarev, G.A. Botton, S.Y. Savrasov, C.J. Humphreys, A.P. Sutton, Electron-energy-loss spectra and the structural stability of nickel oxide: An LSDA+U study, Phys Rev B 57 (1998) 1505–1509. https://doi.org/10.1103/PhysRevB.57.1505.
[24] W. Chen, Y. Tang, G. Zhao, D. Teng, H. Chai, Z. Feng, X. Dai, Gas adsorption induces the electronic and magnetic properties of metal modified divacancy graphene, J. Phys. Chem. Solids 136 (2020) 109151. https://doi.org/10.1016/J.JPCS.2019.109151.
[25] J. Yang, Y. Fan, P.F. Liu, Theoretical insights into heterogeneous single-atom Fe1 catalysts supported by graphene-based substrates for water splitting, Appl. Surf. Sci. 540 (2021) 148245. https://doi.org/10.1016/j.apsusc.2020.148245.

Graphical abstract

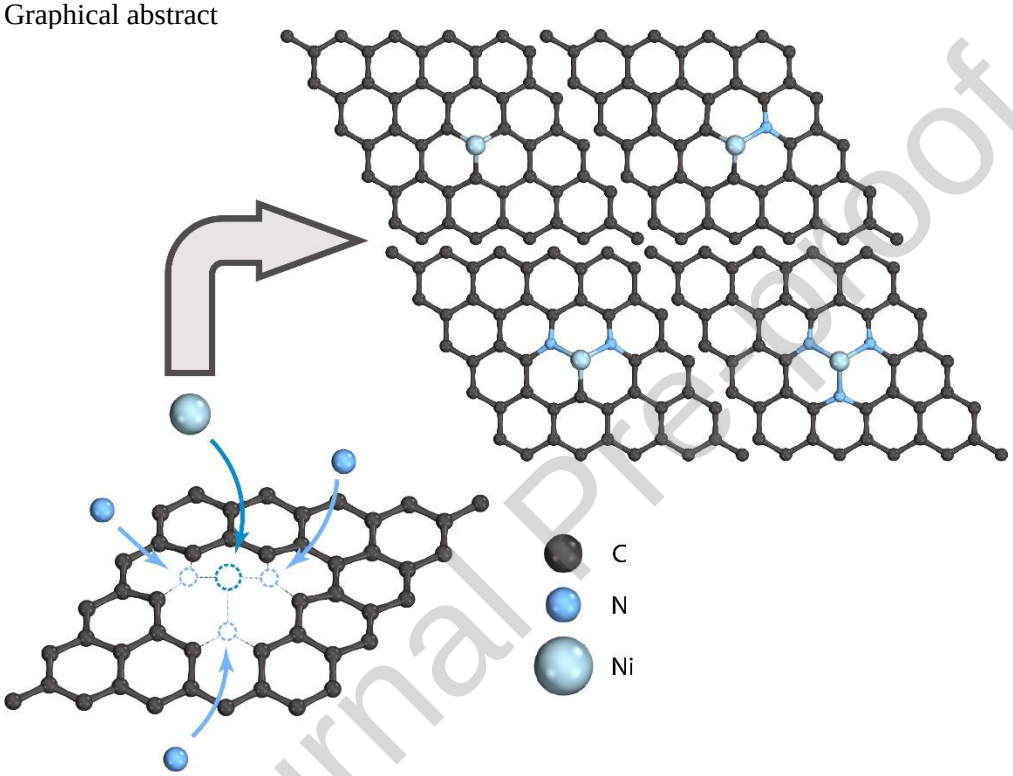

Author statement

Data acquisition, methodology, data curation and formal analysis (H. Cabrera-Tinoco, L. Borja-Castro and R. Valencia-Bedregal), conceptualization, interpretation, validation, data curation and visualization (A. Perez-Carreño, J. Albino Aguiar, N.O. Moreno, S.N. Holmes, C.H.W. Barnes and L. De Los Santos Valladares) and all authors have contributed to write and correct the manuscript.

Declaration of Competing Interest

The authors declare no competing interested.